PROCEEDINGS OF SCIENCE

Vertex reconstruction and tracking performance of the STS detector with the mCBM setup at SIS18

Dario Alberto Ramirez Zaldivar
(CBM Collaboration)[a,b]

[a] *GSI Helmholtzzentrum für Schwerionenforschung, Planckstr 1, 64291 Darmstadt, Deutschland*
[b] *Goethe University, Frankfurt, Deutschland*

E-mail: d.ramirez@gsi.de

The Compressed Baryonic Matter (CBM) experiment is one of the experimental pillars at the Facility for Antiproton and Ion Research (FAIR). The Silicon Tracking System (STS) is the central detector for track reconstruction and momentum measurement. It is designed to measure heavy ion collisions at interaction rates up to 10 MHz. It comprises approximately 900 double-sided silicon strip sensors with 1024 strips per side, arranged in 8 tracking stations in a magnetic field of 1 T · m. In the context of the FAIR Phase-0 program, the mCBM setup at SIS18/GSI is a small-scale precursor of the full CBM experiment, consisting of pre-series productions of all major CBM detector subsystems aiming to verify CBM's concepts of free-streaming readout electronics, data transport, and online reconstruction. The mini-STS (mSTS) setup consists of 11 sensors arranged in 2 stations and no magnetic field.

Heavy ion collisions in the $1 - 2$ AGeV$/c$ range were measured with an average collision rate of 500 kHz. The primary vertex is reconstructed using the two layers of the mSTS detector by tracks reconstructed as straight lines. Hit reconstruction efficiency was estimated using correlations with downstream detectors.

The 32nd International Workshop on Vertex Detectors (VERTEX2023)
16-20 October 2023
Sestri Levante, Genova, Italy

© Copyright owned by the author(s) under the terms of the Creative Commons Attribution-NonCommercial-NoDerivatives 4.0 International License (CC BY-NC-ND 4.0).

PoS(VERTEX2023)064

1. Introduction

The Silicon Tracking System (STS) is the core detector for tracking and momentum determination of charged particles in the CBM experiment [1]. It is designed to reconstruct the trajectories of up to 1000 charged particles per event with high efficiency; it is expected to achieve a momentum resolution better than 2% and to reconstruct complex event topologies, such as the weak decays of strange or charmed hadrons and hypernuclei. To reach event rates of up to 10 MHz, it uses fast and radiation-hard components, self-triggered front-end electronics, and a free-streaming readout architecture. A general detector description is given in [2, 3].

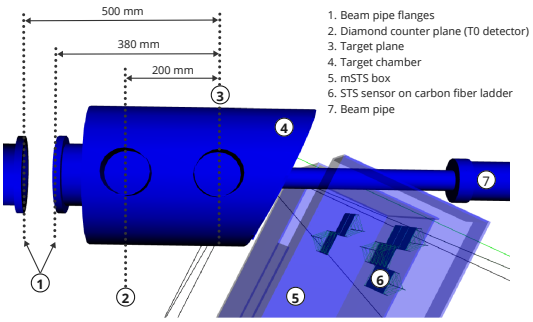

Figure 1: Target Chamber scheme of the mCBM setup highlighting the planes of interest for secondary interaction points.

Prototype or pre-series components of all major CBM systems are installed in a common test setup, mini-CBM (mCBM), at the SIS18 synchrotron (GSI). The goals of mCBM focus on testing and optimizing the operation as a full system under realistic experimental conditions [4]. During beamtime campaigns in 2021 and 2022, heavy ion collisions (O+Ni, Ni+Ni, Au+Au) were measured at 2 AGeV/c, with an average collision rate of 500 kHz. In addition, several detector tests with higher interaction rates were performed.

The mini-STS(mSTS) setup consists of 11 modules: two with 62 × 124 mm^2, 9 with 62 × 62 mm^2 silicon sensors, arranged in four physical units. The system is laid out in 2 tracking stations of 12 × 12 cm^2 and 18 × 18 cm^2. A sketch top view of the mSTS and mCBM target chamber setup is shown in Fig. 1.

2. Data processing and testing

Prior to the installation in the mCBM cave, an energy calibration was performed to adjust the dynamic range of the ADC using a calibrated internal pulse generator and dedicated counters in the STS custom-designed front-end electronic [5]. The estimated baseline noise level corresponds to an Equivalent Noise Charge (ENC) below the targeted system noise of 1000 e. Six modules in the first three physical units, located in the first tracking station and the central ladder of the second tracking station, were operated with relatively low thresholds, around $3-4\sigma$. On the other hand, the 5 modules located in the side ladders of the second tracking station were operated with high threshold values due to the considerable noise in the physical unit. The typical particle rates were up to 28 kHz/channel.

The simplest decoded information from the recorded data files is the *StsDigi*: containing the address (module) and channel of the fired strip and time and charge information of the signal. Similar classes for all detection subsystems exist adapted to the particularities of each detector. The STS *Clusters* are reconstructed by correlating signals from neighboring fired strips [6]. *Hits* are finally derived from the correlation of clusters on the p- and n-side [7] and fed to the tracking

PoS(VERTEX2023)064

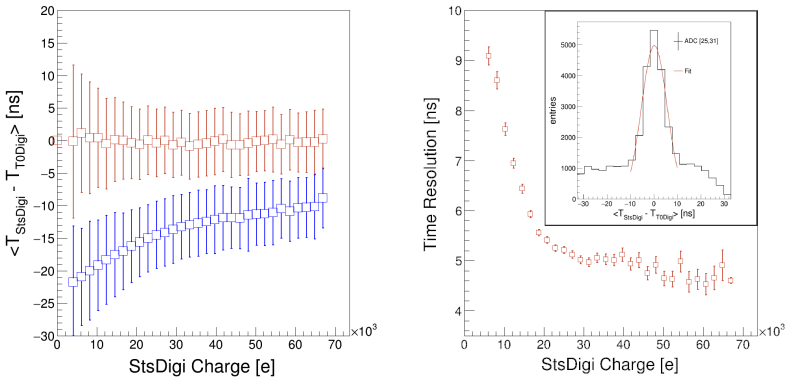

(a) (b)

Figure 2: a) Signal amplitude dependence of the time delay of STS signals with respect to T0, with(red) and without(blue) correction. b) Time resolution dependence on the STS signal amplitude and y-projection for charge $> 40 \cdot 10^3$ e.

algorithm [8]. *Events* are defined using a seed detector and including all Digis within a time window, i.e., 60 ns for the STS. As a seed, a small diamond detector (T0) was used and placed in the beam upstream of the target. Typically, it is required that there is only one T0 hit to avoid event pile-up; a minimum number of 8 TOF signals is required to remove empty or single-noise events, while events with more than 50 STS signals are removed to suppress massive pick-up noisy events.

Before cluster, hit, and event reconstruction, time calibration is applied to raw signals. The time calibration corrects for potential offsets in the individual detector systems and for the time walk effect, i.e., the delay of the signal for lower signal amplitude. Fig. 2(a) shows the delay of the STS signal with respect to T0 as a function of the signal amplitude; before (blue) and after (red), the time walk correction is performed. The purpose of the left panel is to quantify the impact of the walk effect in terms of signal delay and signal resolution. The systematic uncertainty is negligible with respect to the resolution: $< 1\%$. Therefore, the vertical bars represent the width of the distribution. The calibration ensures a proper synchronization within the detector resolution, which ranges between 4.6 and 9.2 ns, as shown in Fig. 2(b).

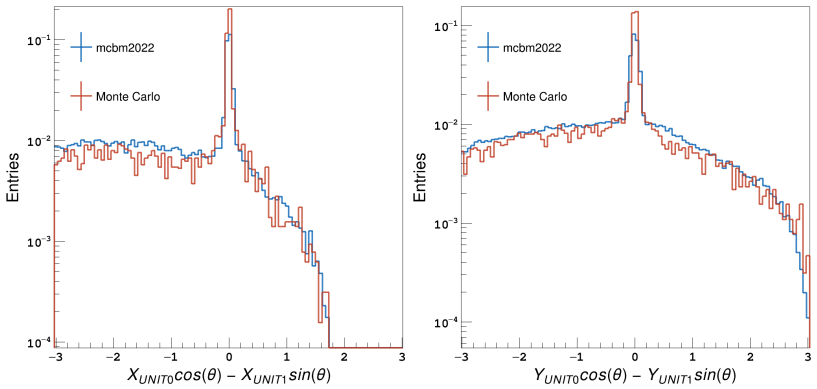

Figure 3: Reconstructed hit position correlation between mSTS tracking stations. Comparison of the correlation peak between Monte Carlo and mCBM2022 data.

The space resolution is studied using the correlations of the hit position in the two tracking stations. The projection of the correlation peak is shown in Fig. 3. The width of the correlations is narrower in X (500 µm) than in Y (800 µm) direction since the sensor pitch follows the X coordinate,

PoS(VERTEX2023)064

while in Y is tilted by a stereo-angle of 7.5°. Although the correlations are dominated by the large transversal spread of the beam, the figure demonstrates an excellent agreement with Monte Carlo simulation.

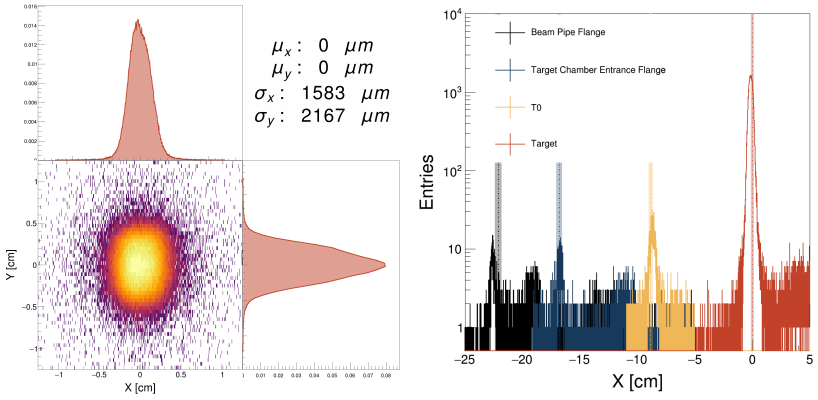

(a) (b)

Figure 4: a) Beam spot reconstruction at the target plane by STS tracks. b) Projection along the x-axis for different z-planes, corresponding to secondary interaction points.

As there is no magnetic field in the setup, the event vertex is reconstructed by building straight lines from the hits in the two STS stations. To reduce background and false combinations, events with low multiplicity are chosen, and only STS signals with amplitude larger than 20 ke are used. Vertex reconstruction is performed independently with STS track-lets, where the intense region close to $(X;Y) : (0;0)$ corresponds to the beam's interaction with the Ni target.

The vertex reconstruction allows the identification of secondary interaction points of the beam with different elements of the Target Chamber, shown in Fig. 1. The X projections of STS track-lets at different z-planes are shown with different colors in Fig. 4(b). The dashed lines and the shadow boxes represent the expected position of such peaks, in remarkably good agreement with the measurement. The reconstructed vertex at the Ni target plane and the X, Y projections, shown in Fig. 4(a), is fitted, resulting in a beam profile at the target plane of $\sigma^X_{trg} = 0.1583(4)$ cm, $\sigma^Y_{trg} = 0.2167(13)$ cm. The beam spot x-profile is compatible with information extracted from the channel distribution measured by the T0 detector, resulting in a beam profile with approximately 0.15 cm width along the x-axis. The strip along the y-axis for the T0 detector was non-operational.

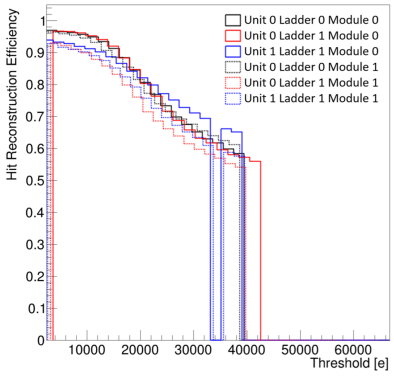

Figure 5: Hit reconstruction efficiency as a function of strip charge threshold.

3. Hit Reconstruction Efficiency

The STS hit reconstruction efficiency (HRE) is studied using track-lets formed by one hit in one of the STS stations and a hit in a downstream detector (TOF) as a reference. Only hit pairs originating from a narrow region around the beam spot are used to reduce false combinations. The hit in the STS is considered found if it is reconstructed in a 3 σ window around the expected

PoS(VERTEX2023)064

extrapolated position. This procedure, verified with simulations where the efficiency can be derived from Monte Carlo information, leads to an approximate value of 97% in the detector active areas for the modules operated with $3-4\ \sigma$ threshold. In the offline analysis, the strip charge threshold is progressively increased, and digis below this threshold are discarded from further analysis. Fig. 5 shows the hit reconstruction efficiency as a function of the threshold for six different modules (four in the first station and two in the central ladder of the second station). As expected, the HRE decreases as the threshold increases from the lowest value used in the beamtime towards higher values (MIP are around 24000 e). This cut would have a tracking efficiency of $\sim 60\%$ or less, but for the purpose of vertex reconstruction, we wanted to maximize the purity of the signal.

4. Summary

The mSTS detector, which employs two tracking stations in the study of heavy-ion collisions at SIS18, facilitates an evaluation indicating the feasibility of attaining the targeted performance level for the STS system. The system manifests commendable spatial and temporal resolution, proficient vertex capabilities, and hit reconstruction efficiency.

References

[1] K. Agarwal for the CBM Collaboration. The compressed baryonic matter (cbm) experiment at fair—physics, status and prospects. *Physica Scripta*, 2023. doi: 10.1088/1402-4896/acbca7.

[2] H. R. Schmidt. The silicon tracking system of the cbm experiment at fair. *Nuclear Instruments and Methods in Physics Research Section A: Accelerators, Spectrometers, Detectors and Associated Equipment*, 2019. doi: https://doi.org/10.1016/j.nima.2018.09.094. Frontier Detectors for Frontier Physics: 14th Pisa Meeting on Advanced Detectors.

[3] A. Rodriguez Rodriguez. The silicon tracking system of cbm: towards tests with heavy ion collisions. *2019 IEEE Nuclear Science Symposium and Medical Imaging Conference (NSS/MIC)*, 2019. doi: 10.1109/nss/mic42101.2019.9059911.

[4] C. Sturm, D. Emschermann, and N.Herrmann. Achievements of the mcbm beam campaign 2022, cbm progress report 2022. Technical report, 2022.

[5] A. Rodríguez Rodríguez et. al. Functional characterization of modules for the silicon tracking system of the cbm experiment. *Nuclear Instruments and Methods in Physics Research Section A: Accelerators, Spectrometers, Detectors and Associated Equipment*, 2024. doi: https://doi.org/10.1016/j.nima.2023.168813.

[6] V. Friese. A cluster-finding algorithm for free-streaming data. *EPJ Web of Conferences*, 2019. doi: 10.1051/epjconf/201921401008.

[7] H. Malygina. *Hit reconstruction for the Silicon Tracking System of the CBM experiment*. PhD thesis, Universitätsbibliothek Johann Christian Senckenberg, 2018.

[8] V. Akishina and I. Kisel. Online 4-dimensional reconstruction of time-slices in the cbm experiment. *IEEE Transactions on Nuclear Science*, 2015. doi: 10.1109/TNS.2015.2498099.

PoS(VERTEX2023)064